

ORIGINAL RESEARCH PAPER

Oxytetracycline photodegradation by transition metals doped ZnO nanorods

Siavash Fathi, Bagher Aslibeiki*, Reza Torkamani

Faculty of Physics, University of Tabriz, Tabriz, Iran

Received: 2023-03-11

Accepted: 2023-04-06

Published: 2023-08-10

ABSTRACT

In recent decades, pollution increases in water resources endanger human life and other living organisms. Researchers have applied different methods to eliminate water contaminants. Photocatalytic is one of these methods that have been used widely for wastewater treatment. In this study, a series of Mn, Fe, Co, Ni, and Cu-doped ZnO nanorods were applied as visible-light-activated catalysts for oxytetracycline (OTC) degradation. Characterization of the nanorods was performed using XRD, FE-SEM, UV-Vis, and PL techniques. The results demonstrate that the photocatalytic activity of the samples highly depends on the morphology, size, and band gap energy. The UV-Vis spectroscopy indicates that Fe doping has reduced the band gap energy to 2.91 eV. The variation of the band gap permits the absorption of low-energy photons and the excitation of valence band electrons. The photoluminescence spectra reveal that doping has an effective role in inhibiting the recombination of electron/hole pairs during the photocatalytic process. The Mn-doped sample exhibits significantly increased photocatalytic activity and greater degradation rate constant (k) in comparison with the pure ZnO.

Keywords: Zinc oxide, Nanorods, Transition metal doping, Photocatalytic degradation, Oxytetracycline.

How to cite this article

Fathi S., Aslibeiki B., Torkamani R., Oxytetracycline photodegradation by transition metals doped ZnO nanorods. J. Water Environ. Nanotechnol., 2023; 8(3): 254-266. DOI: 10.22090/jwent.2023.03.005

INTRODUCTION

Zinc oxide, abbreviated ZnO, is a n-type semiconductor. This implies that the conduction band is essentially teeming with electrons, giving birth to an abundance of intriguing optical and electrical features. The most remarkable is its bandgap energy of 3.37 eV, which gives it the rare ability to absorb UV radiation while remaining completely transparent in the visible spectrum. At room temperature, its exciton binding energy is 60 MeV, which is relatively high. This is in sharp contrast to other semiconductors that are more widely utilized, such as silicon and gallium arsenide, whose exciton binding energies are quite low. It is also a chemically stable molecule that may thrive

in extremely unfavorable settings. Its durability makes it appropriate for a wide range of electronic and industrial applications. Besides, it has been synthesized in different nanostructures, such as nano combs [7, 8], nanotubes [9], nano springs [10], nanorods [11], nanorings [12], nanowires [13], nanoflowers [14] and every one of them has different applications. Among them, nanorods due to their unique properties, such as a high aspect ratio, a large surface area, biocompatibility, photocatalytic properties, high electron mobility, and distinctive electrical and electrochemical properties, have diverse applications in fields such as medicine, the environment and the electronic industry [15-22]. Doping has the potential to influence the crucial characteristics of ZnO, such

* Corresponding Authors Email: b.aslibeiki@tabrizu.ac.ir



This work is licensed under the Creative Commons Attribution 4.0 International License.

To view a copy of this license, visit <http://creativecommons.org/licenses/by/4.0/>.

as its morphological and optical properties, making it suitable for a diverse range of applications. Cu-doped ZnO nanorods have been shown to have high photocatalytic and sonocatalytic activity in the degradation of water contaminants like methylene blue (MB) and chromium (VI) from aqueous solutions. Cu-doped ZnO nanorods can also be used for water disinfection due to their antibacterial properties [16, 17, 23-25]. Co-doped ZnO nanorods illustrated unique magnetic and semiconducting properties that made them useful for a variety of applications like UV photodetectors and magnetic field sensors [26-28]. Ni-doped ZnO nanostructures have shown promising results in a range of applications including electrical device use. Because Ni-doped ZnO nanostructures have a critical attribute known as long-term current stability, electron-emitter devices can benefit from utilizing these materials [29]. In applications involving humidity sensing, Fe-doped ZnO nanorods have also demonstrated outstanding performance [30, 31]. Moreover, Mn-doped ZnO nanorods displayed outstanding stability and reusability in photocatalytic degradation activities, making them appropriate for applications requiring long-term and sustainable environmental remediation [32]. Among all nanostructure synthesis techniques, the hydrothermal method is a simple, cheap, and environmentally friendly way to create pure and doped ZnO nanostructures that yield high-quality, homogeneous nanostructures at low temperatures. Doped ZnO nanostructures can be made by adding the correct dopant ions into the precursor solution. For preparing pure and doped ZnO nanorods, the hydrothermal method has the advantage of being more easily accessible than chemical vapor deposition and pulsed laser deposition due to the lower temperatures and pressures required for their execution. The hydrothermal approach shows promise as a means of preparing doped ZnO nanostructures with a range of dopant ions for use in fields as diverse as environmental remediation, electronics and sensing [33, 34]. The effect of doping with transition metals (TM) on the structural, morphological and optical properties of ZnO nanorods will be investigated in detail.

EXPERIMENTAL

Materials

Zinc acetate dihydrate ($\text{Zn}(\text{CH}_3\text{COO})_2 \cdot 2\text{H}_2\text{O}$), Zinc nitrate tetrahydrate ($\text{Zn}(\text{NO}_3)_2 \cdot 4\text{H}_2\text{O}$),

Manganese (II) nitrate tetrahydrate ($\text{Mn}(\text{NO}_3)_2 \cdot 4\text{H}_2\text{O}$), Iron (III) nitrate nonahydrate ($\text{Fe}(\text{NO}_3)_3 \cdot 9\text{H}_2\text{O}$), Cobalt(II) nitrate hexahydrate ($\text{Co}(\text{NO}_3)_2 \cdot 6\text{H}_2\text{O}$), Nickel(II) nitrate hexahydrate ($\text{Ni}(\text{NO}_3)_2 \cdot 6\text{H}_2\text{O}$), Copper(II) nitrate trihydrate ($\text{Cu}(\text{NO}_3)_2 \cdot 3\text{H}_2\text{O}$), Hexamethylenetetramine ($\text{C}_6\text{H}_{12}\text{N}_4$) and Ethanol (99%) manufactured by Merck company.

Preparing the seed layers

First, the quartz substrates were cleaned for 20 min with an ultrasonic cleaner, ethanol, and acetone. Later on, to prepare seed layers, we made a zinc acetate dihydrate and ethanol solution with a concentration of 5 mM. The spin-coating approach was used to deposit the seed layers on the substrates, repeating the process six times for each sample at a speed of 2000 rpm for 30 seconds. The samples were spin-coated six times, dried for 15 min at 110 °C each time then all of the samples were annealed at 350 °C.

The growth of nanorods on the seed layer

After making the seed layers, we used deionized water as a solvent for the pure ZnO sample to make a solution of Zinc nitrate tetrahydrate and Hexamethylenetetramine with a molar ratio of 1:1. For other samples, we used Manganese (II) nitrate tetrahydrate, Iron(III) nitrate nonahydrate, Cobalt(II) nitrate hexahydrate, Nickel(II) nitrate hexahydrate, Copper(II) nitrate trihydrate as sources of Mn, Fe, Co, Ni, Cu doping and the atomic concentration ratio of all elements to Zn were 6 mol %. The optimal conditions for the preparation of nanorods were obtained from the scientific literature [35]. All growth solutions for pure and other doped samples were stirred for 30 min to get a homogenous solution. Then, the seed layers were placed in pure and doped growth solutions inside an autoclave reactor. Subsequently, the autoclave reactor was placed in the oven for 3 hours at 90 °C for each sample. After that, pure and doped samples were taken out of the autoclave and oven and annealed in a furnace at 400 °C. The whole process of the nanorods preparation, from the first step of the seed layer preparation to the doping stage with transition metals, is shown in Fig. 1. For the X-ray diffraction test, we used a Tongda TD-3700 device with wavelength radiation ($\lambda = 1.5406 \text{ \AA}$) in the range of ($2\theta = 20 - 80^\circ$). Morphological and structural properties of all pure and doped

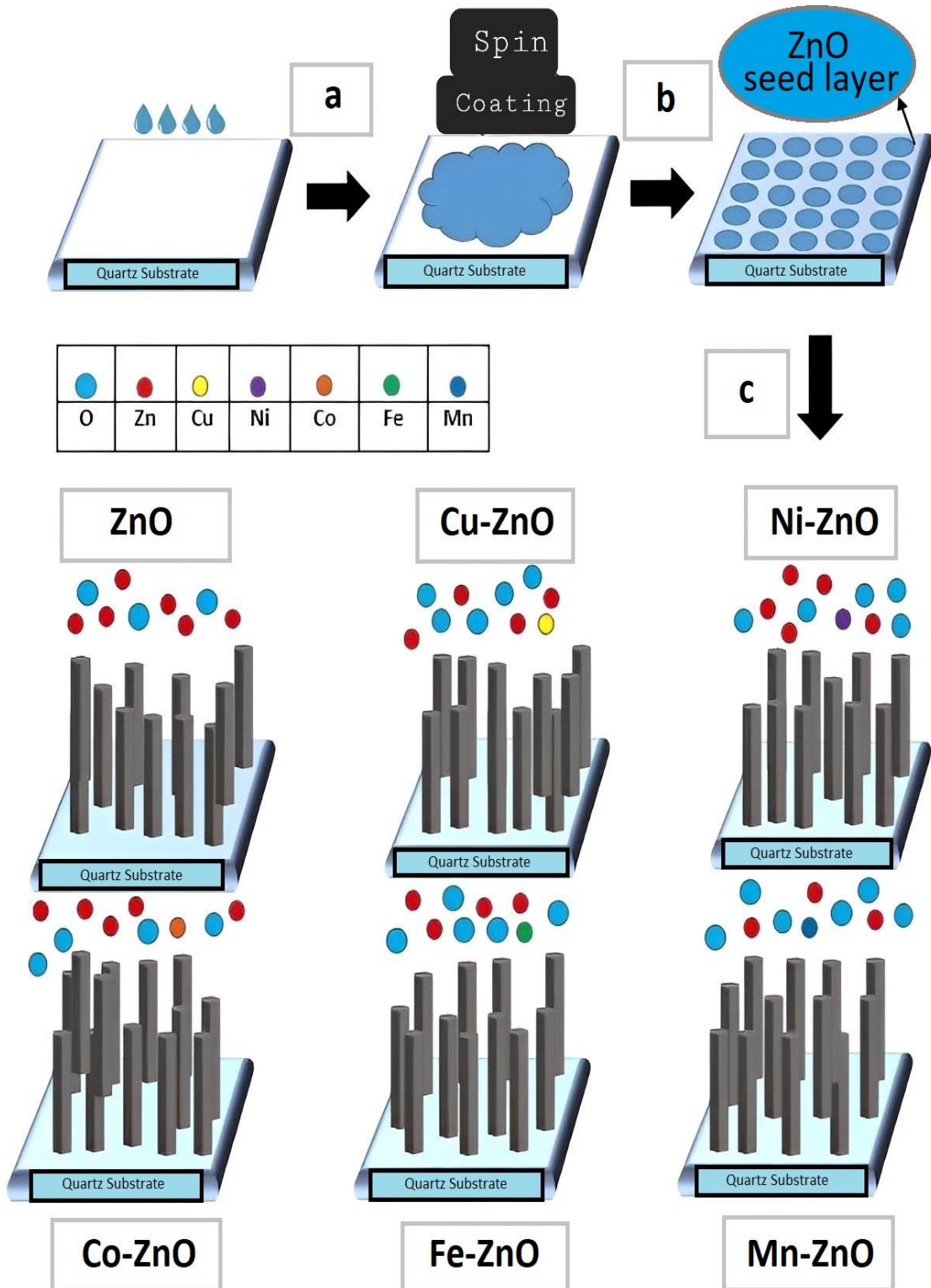


Fig. 1. (a) Schematic representation of the ZnO seed layer solution, (b) spin coating and (c) the growth process of ZnO nanorods

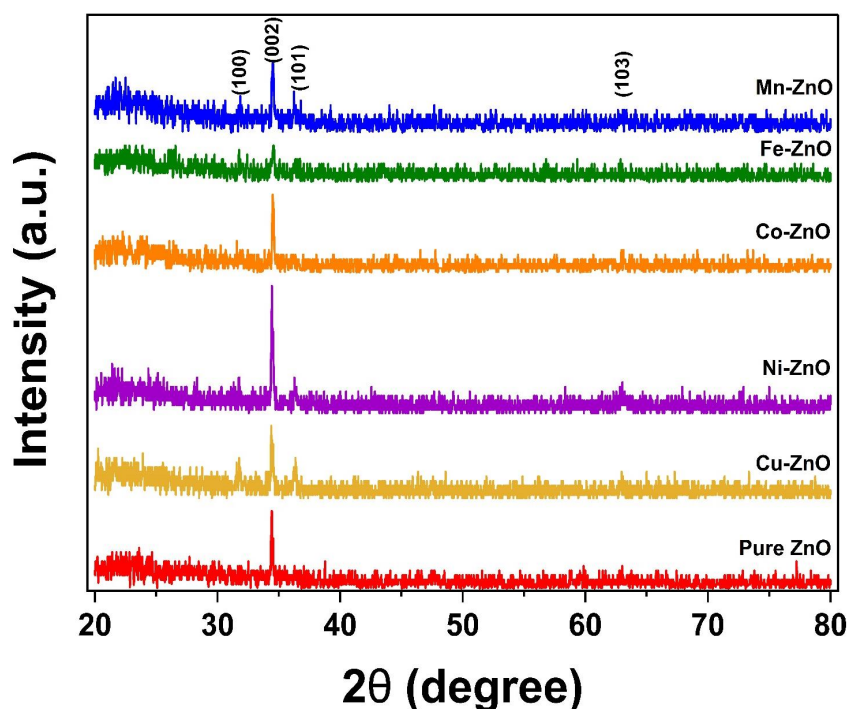


Fig. 2. XRD patterns of pure and TM-doped ZnO nanorods

samples were studied using a field emission scanning electron microscope (MIRA3-TESCAN). The optical properties of all the pure and doped samples were analyzed by a photometer (JASCO FP-6200) with a 320 nm excitation wavelength.

Process of photocatalytic degradation

The photocatalytic degradation of OTC in an aqueous suspension under visible light was used to evaluate the photocatalytic activity of pure and TM-doped ZnO nanorods. Initially, a 5 ppm OTC aqueous solution was formulated. Afterward, samples were suspended in an aqueous solution. 180 min were spent exposing a catalyst solution suspension to visible light. The solution was sampled at various 30 min intervals and examined using UV-Vis spectroscopy and absorption spectra.

RESULTS AND DISCUSSION

The structural study of the samples

X-ray diffraction (XRD) is a standard method for analyzing the crystallinity of materials. The XRD pattern reveals the crystal structure of the material by depicting how X-rays scatter off the atoms in the sample. The first broad peak exhibited between 20 and 30° in Fig. 2, is attributable to the amorphous

glass substrate. The indices (100), (002), (101), and (103) correspond to the Bragg peaks seen at 31.8, 34.49, 36.26 and 62.88°. These peaks are indicative of the presence of a crystalline phase with a wurtzite crystal structure and are characteristic of both pure and doped ZnO nanorods. The position and intensity of these peaks provide information regarding lattice parameters and crystal structure orientation. Specifically, the Bragg peaks seen for Co-doped, Ni-doped, and Cu-doped ZnO nanorods suggest that these dopants have been integrated into the crystal lattice and are occupying certain positions within the crystal structure. The disappearance of the Bragg peak at 62.88° for Mn-doped ZnO and Fe-doped ZnO nanorods suggests that these dopants affect the crystal structure of ZnO differently. The absence of additional peaks linked to metallic oxides of Mn, MnO, Fe, FeO, Co, CoO, Ni, NiO, Cu, CuO, and other impurity phases is indicative of the incorporation of doped Mn, Fe, Co, Ni, and Cu ions into the ZnO lattice. This indicates that the dopants have been successfully incorporated into the crystal structure of the ZnO nanorods without the formation of a distinct phase of metallic oxides. The absence of these additional peaks further verifies that the

Table 1. Crystallite size D_{XRD} , mean diameter D_{SEM} and mean length L_{SEM} of nanorods. The PL peak position (NBE) and band gap energy (E_g) of the samples.

Parameter	Pure ZnO	Cu - ZnO	Ni - ZnO	Co - ZnO	Fe - ZnO	Mn - ZnO
$\langle D \rangle_{XRD} (nm)$	41.6	39.6	46.2	52	39.6	36.2
$\langle D \rangle_{SEM} (nm)$	114.6	110.51	94.38	106.38	107.22	91.44
$\langle L \rangle_{SEM} (nm)$	798.15	412.41	501.57	703.02	845.14	436.86
NBE (nm)	384.63	392.12	388.52	389.80	394.23	392.48
Band gap (eV)	3.24	3.29	3.11	3.28	2.91	3.16

XRD patterns observed for pure and doped ZnO nanorods conform to the hexagonal wurtzite crystal structure, following the standard ICDD cards (card no. 96-901-1663). This suggests that the doping technique did not appreciably affect the crystal structure of the ZnO nanorods and that the dopants are evenly distributed inside the ZnO host lattice. The absence of extra peaks associated with metallic oxides and the confirmation of the hexagonal wurtzite structure of pure and doped ZnO nanorods are both favorable signals of successful dopant incorporation and high crystal quality. The nanorods are preferentially aligned along the c-axis, which is perpendicular to the substrate surface, as indicated by the high intensity of the (002) diffraction peaks for all samples. This indicates that the c-axis, which is a common development direction for ZnO nanorods, controls the growth of the nanorods to a significant degree. The Scherrer equation is a widely employed method for estimating the crystallite size of a substance based on its XRD pattern. With this equation, one may determine the crystallite sizes of Mn^{2+} , Fe^{2+} , Co^{2+} , Ni^{2+} , and Cu^{2+} doped ZnO. The Scherrer equation establishes a relationship between the FWHM of a diffraction peak and the size of the crystallites [31, 36, 37]:

$$\langle D \rangle = \frac{K\lambda}{\beta \cos\theta} \quad (1)$$

Where D is the crystallite size, K is the Scherrer constant (typically around 0.9), λ is the X-ray wavelength, β is the FWHM of the peak and θ is the Bragg angle. The average size of crystallites estimated from XRD patterns of pure and doped ZnO with Mn, Fe, Co, Ni, and Cu is shown in Table 1. These samples had respective average diameters of 41.6, 36.2, 39.6, 52, 46.2 and 39.6 nm.

The morphological study of the samples

The morphologies of both pure and TM-doped ZnO nanorods were analyzed using field emission scanning electron microscopy. The length and cross-sectional views of these nanorods are depicted in Fig. 3, FE-SEM images and a long-normal function (Eq. 2) were utilized to calculate the diameters and lengths of pure ZnO and doped nanorods:

$$f(D) = \frac{1}{\sqrt{2\pi}\sigma D} \exp\left[-\frac{\ln^2\left(\frac{D}{D_0}\right)}{2\sigma^2}\right] \quad (2)$$

Where D_0 is the median diameter or length and σ is the distribution. The mean diameter or length is $\langle D \rangle = D_0 \cdot \exp(\sigma^2/2)$ and the standard deviation is $\sigma_D = \langle D \rangle \cdot [\exp(\sigma^2) - 1]^{1/2}$ were calculated using the fit parameters D_0 and σ . The estimated lengths of pure ZnO and ZnO doped with Mn, Fe, Co, Ni, and Cu are 798.15, 436.86, 845.14, 703.02, 501.57, and 412.41 nm, respectively, as shown in Table 1. Fig. 4, displays the estimated nanorod diameters of pure ZnO and ZnO doped with Mn, Fe, Co, Ni, and Cu, which are 114.6, 91.44, 107.22, 106.38, 94.38, and 110.51 nm, respectively. Each nanorod possesses a hexagonal wurtzite structure. The growth direction of the nanorods observed through FESEM corresponds well with the intensity of the (002) peak in the X-ray pattern for both pure and TM-doped ZnO samples. Additionally, the findings indicate that all the pure and TM-doped ZnO nanorods have high crystalline quality. Fe-doped and pure ZnO nanorods had the longest length and largest diameter among the samples, respectively, while Cu-doped and Mn-doped ZnO nanorods had the smallest length and diameter, respectively. The EDX spectra in Fig. 5, depict the sample composition, which included transition metals (Mn, Fe, Co, Ni, Cu, and Zn), oxygen, silicon (from the quartz substrate), and carbon, confirming the existence of transitional elements in the samples.

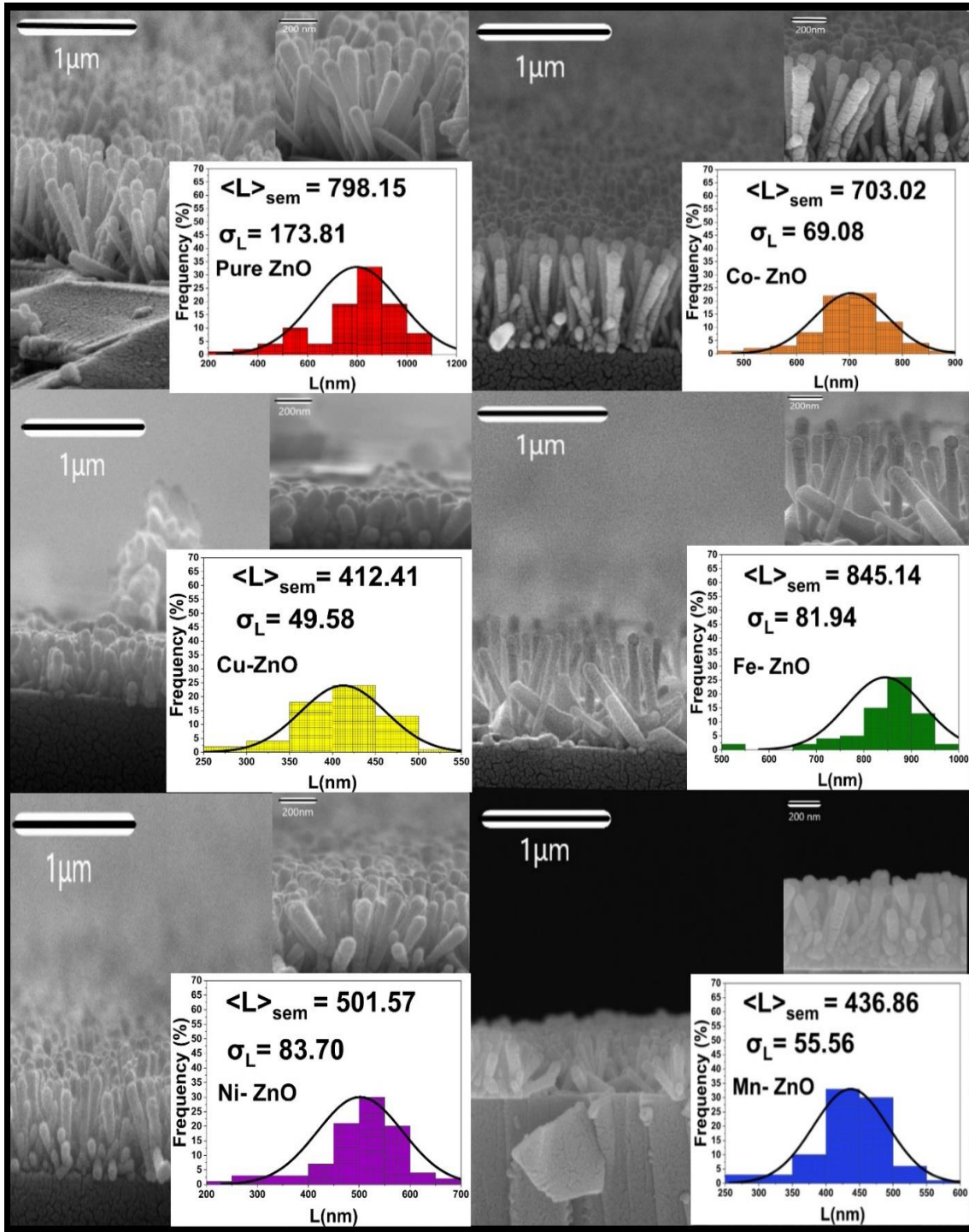


Fig. 3. FE-SEM images of pure and TM-doped ZnO nanorods

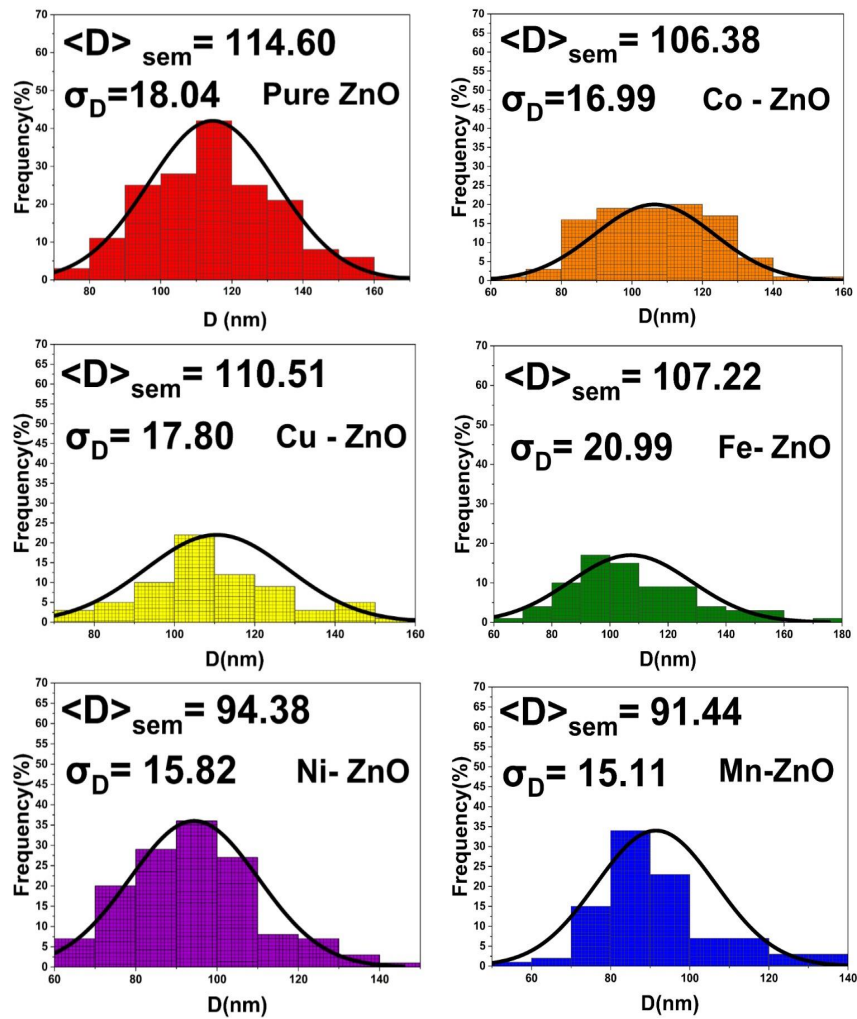


Fig. 4. Diameter of pure and TM-doped ZnO nanorods

The optical properties of the samples

The band gap values of both pure and TM-doped ZnO nanorods are illustrated in Fig. 6. To determine the optical bandgap values of the prepared nanorods, we employed Tauc’s equation (Eq. 3) and analyzed the UV-Vis (DRS) optical absorbance spectra [33, 38]:

$$(\alpha h\nu)^2 = K(h\nu - E_g) \quad (3)$$

Tauc’s equation (Eq. 3) contains the absorption constant (α), the photon energy ($h\nu$), a constant (K), and the band gap energy (E_g). The band gap values of pure and Mn, Fe, Co, Ni, and Cu-doped ZnO are listed in Table 1, ranging from 2.91 eV for Co-doped ZnO to 3.29 eV for Cu-doped ZnO. This suggests that Cu-doped ZnO has the greatest

band gap energy, while Fe-doped ZnO has the lowest. Fig. 7, illustrates Gaussian fitting diagrams of the photoluminescence (PL) spectrum for both pure and TM-doped ZnO nanorods. The corresponding values for different samples are shown in Table 1. The first peak was recorded for pure ZnO at 384.63 nm and for other transition metals (Mn, Fe, Co, Ni, and Cu) doped ZnO was measured at 392.48, 394.23, 389.80, 388.52, and 392.12 nm, respectively, all of which were located in the UV emission zone. The PL strength, corresponding to exciton recombination, was higher in the TM-doped ZnO nanorods than in the pure sample and Fe-doped ZnO exhibited the maximum value among all samples. The second peak was situated in the visible emission zone, ranging from 400 to 700 nm for all samples. The



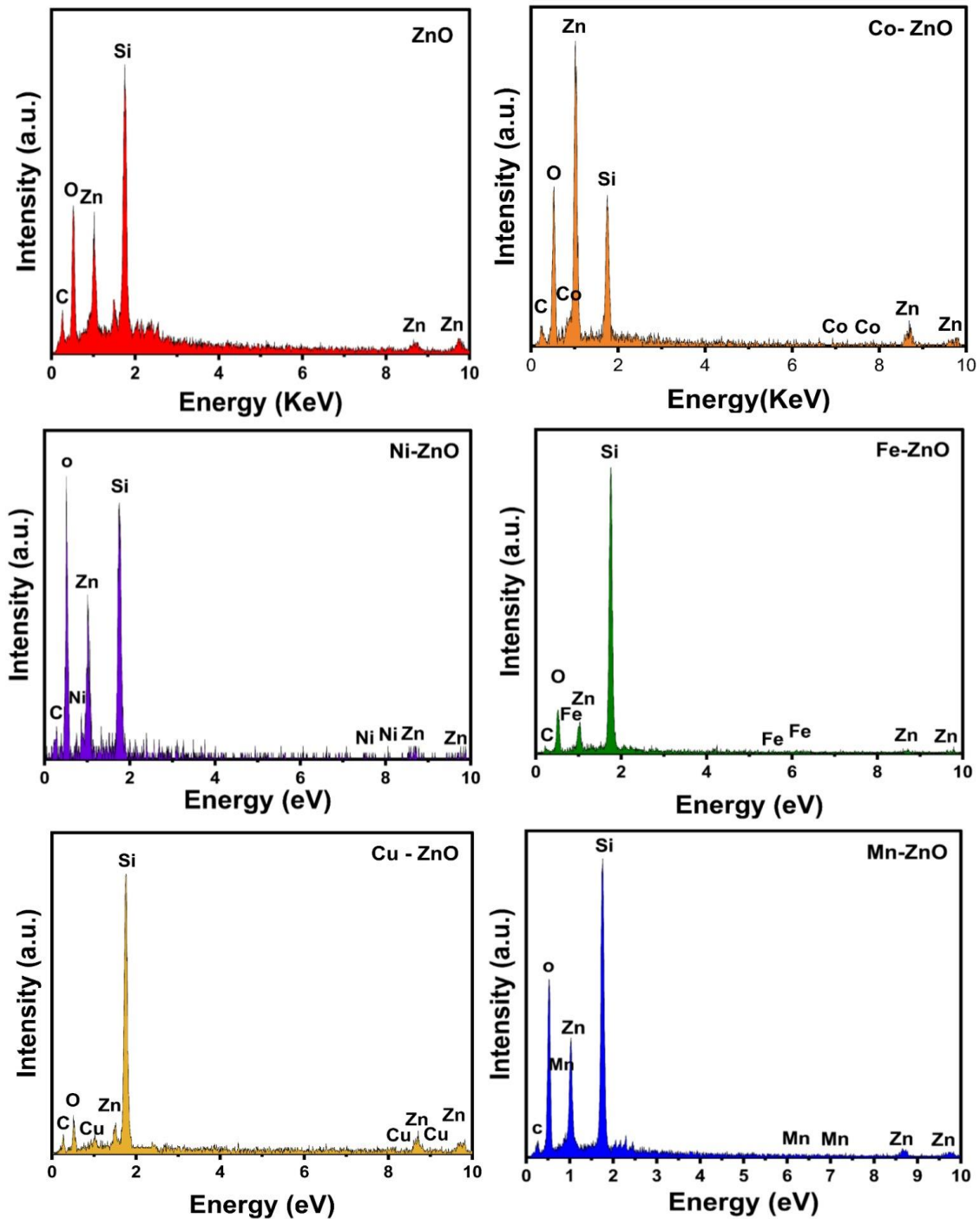


Fig. 5. EDX spectra of pure and TM-doped ZnO nanorods

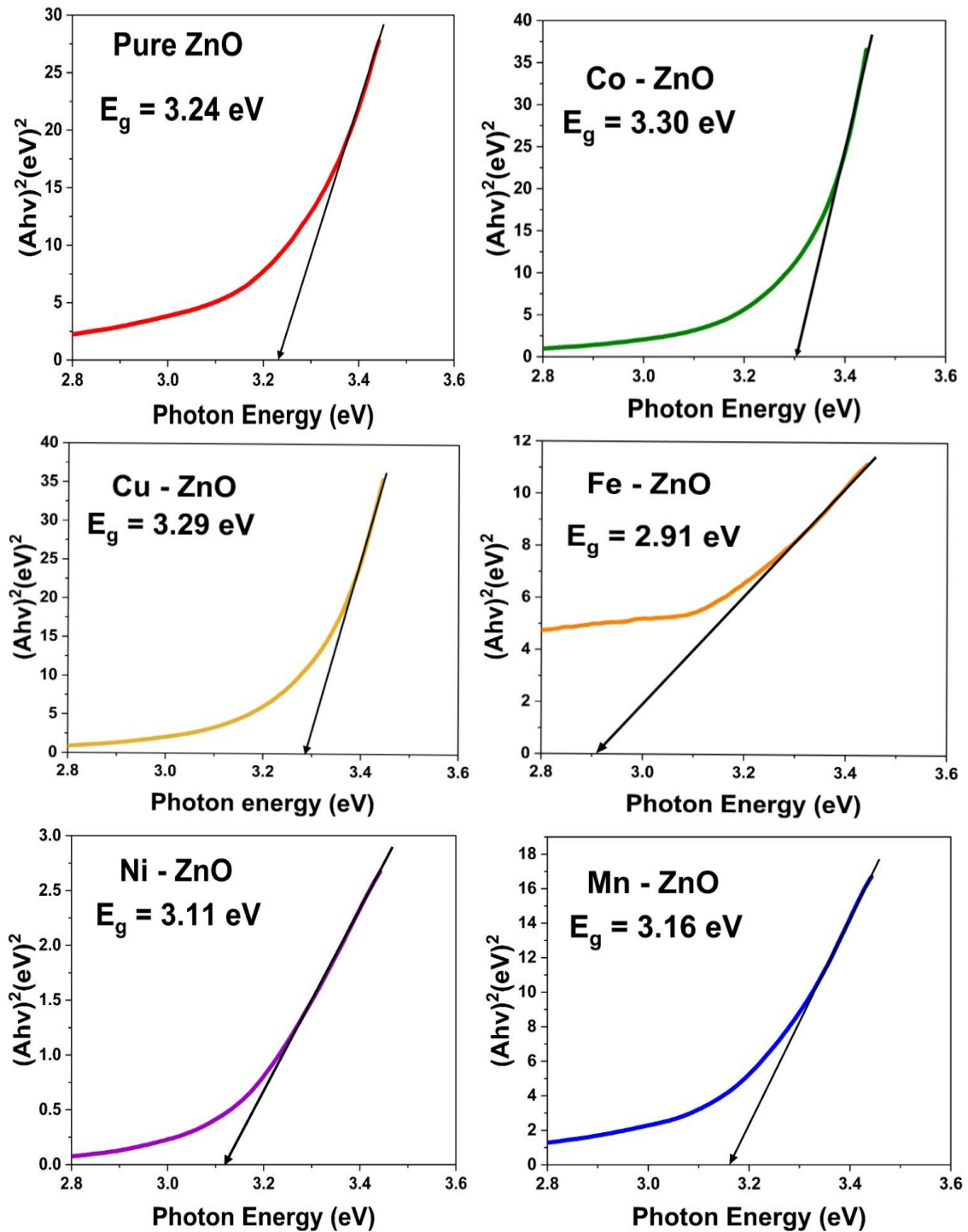


Fig. 6. Photoluminescence (PL) spectra of pure and TM-doped ZnO nanorods

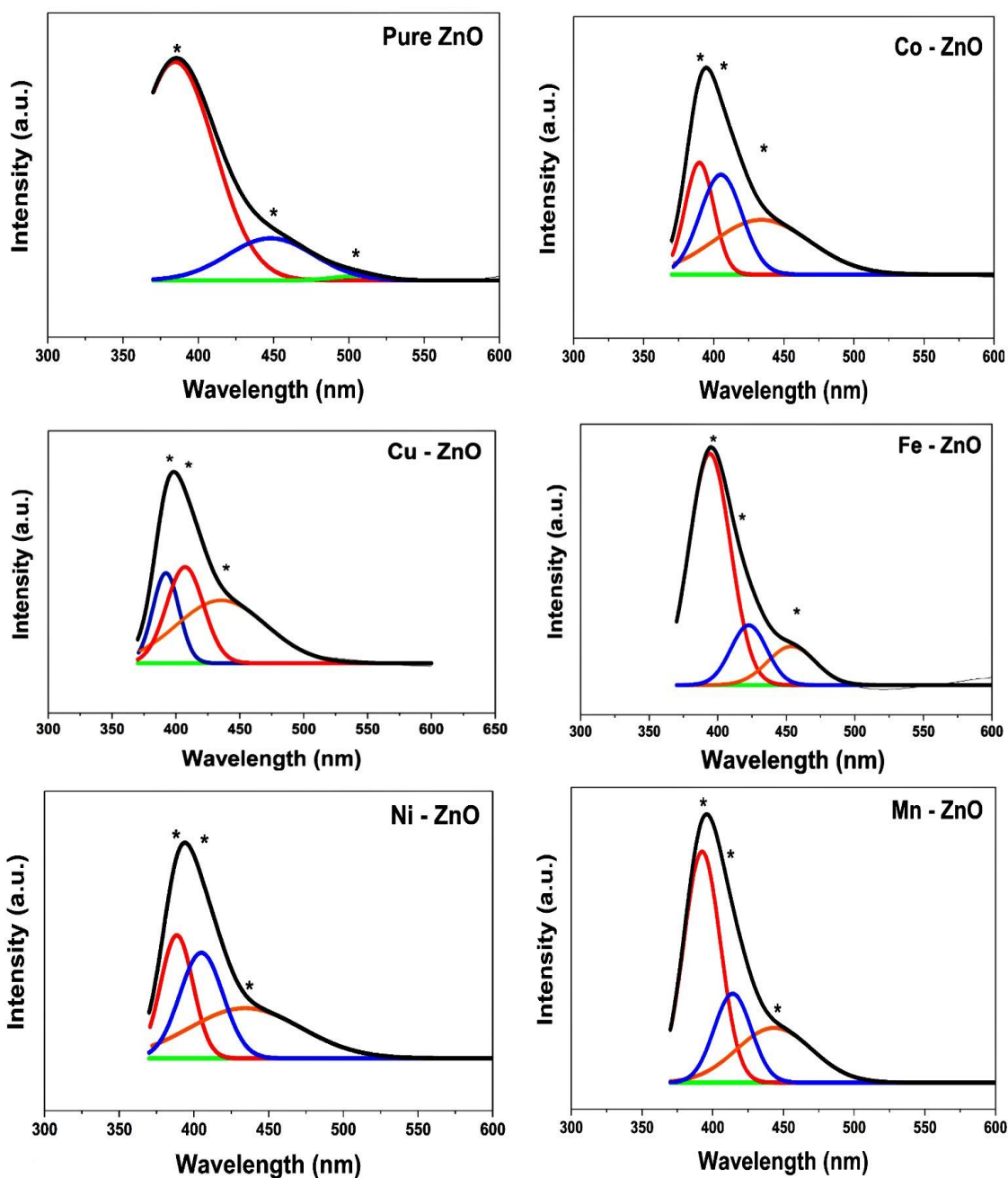


Fig. 7. Tauc plots to estimate the band gap energy (E_g) of pure and TM-doped ZnO nanorods

first peak represents near-band edge emission (NBE) caused by the band-to-band recombination of excitons in the pure and TM-doped ZnO nanorods. The second peak in the visible zone describes deep-level emission (DLE) due to intrinsic defects such as V_{zn} , Z_{ni} and V_o , O_i , as well as extrinsic impurities. Additionally, the intensity of NBE peaks was higher than that of DLE peaks

for all samples, indicating the crystallinity quality of the samples [35].

The photocatalytic activities of the nanorods

The rate of OTC photodegradation by pure and TM-doped ZnO nanorods is depicted in Fig. 8A. The image demonstrates that Mn-doped ZnO nanorods degrade more quickly than pure ZnO

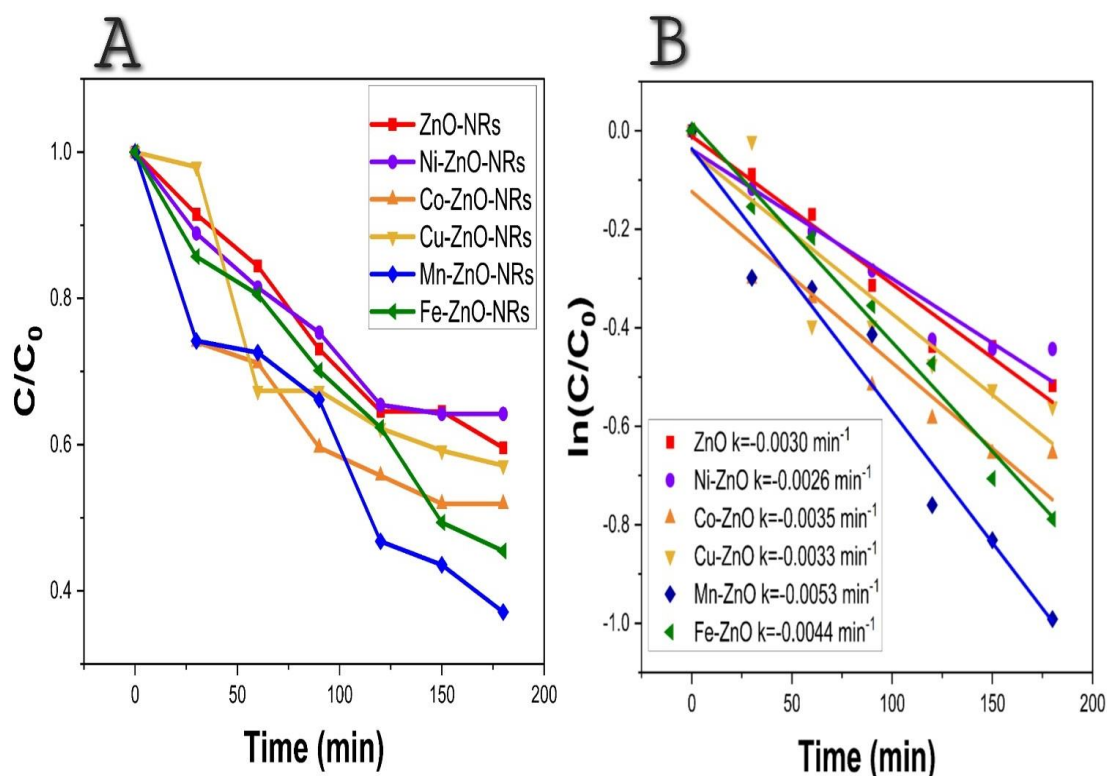


Fig. 8. A) Photocatalytic degradation of OTC by pure and TM-doped ZnO nanorods and B) The kinetic graphs for the pseudo-first-order reaction of OTC by pure and TM-doped ZnO nanorods

nanorods. Pure and Ni-doped ZnO nanorods, on the other hand, display slower degradation rates. To compute the percentage of pollutant degradation, use the following formula:

$$\text{Photodegradation efficiency}(\%) = \frac{C_0 - C}{C_0} \times 100 \quad (4)$$

where C_0 is the initial concentration and C is the OTC concentration after a certain amount of time being exposed to radiation. The photodegradation percentages of samples containing pure ZnO and those doped with Mn, Fe, Co, Ni, and Cu were determined to be 40.42, 62.90, 54.54, 48, 35.80 and 42.85%, respectively. The scientific literature suggests that several factors affect how well a photocatalyst works. Some of these factors are the synergistic effect of metal and zinc, oxygen vacancies, a decrease in size, and a slowing down of the rate at which electron-hole pairs come back together. Based on the FE-SEM images, it has been observed that the average diameter of Mn-doped ZnO nanorods is smaller than that of pure ZnO nanorods. Hence, Mn-doped ZnO nanorods possess a higher surface-to-volume proportion than pure ZnO nanorods. It is well known that a

high surface-to-volume ratio enhances the rate of degradation. As per Fig. 8B, Mn-doped ZnO nanorods demonstrate a faster degradation rate compared to pure ZnO nanorods. Thus, the results derived from FE-SEM pictures and the Scherrer equation have been confirmed. A first-order kinetic model can be utilized to investigate the photocatalytic process:

$$\ln\left(\frac{C}{C_0}\right) = kt \quad (5)$$

The concentration at time t is in mg/L^{-1} is represented by C , while the starting concentration is denoted by C_0 and k denotes the rate constant in min^{-1} . It is a well-known fact that a higher kinetic rate corresponds to better catalytic performance. Fig. 8B displays the k values and according to the graph, the kinetic rate obtained for Mn-doped ZnO nanorods is greater than that of the other samples, indicating their superior catalytic performance [32].

CONCLUSION

This study hydrothermally prepares pure and

TM-doped ZnO nanorods on quartz substrates. (XRD) analysis confirms the incorporation of Mn, Fe, Co, Ni, and Cu ions into the ZnO structure. (FE-SEM) images showed nanorods growing perpendicular to the seed layer. Morphological analysis showed that different elements doped nanorods with different diameters and lengths. By doping ZnO nanorods with transition metals, the energy of the band gap was altered. Gaussian fitting showed that doped ZnO photoluminescence (PL) spectra had stronger ultraviolet zone peaks than pure ZnO. This study assesses the synthesized materials' photocatalytic efficiency, which uses light to start chemical reactions. This study examines how nanorod diameter and length affect photocatalytic efficiency and oxytetracycline degradation. Mn-doped nanorods were the best photocatalysts.

CONFLICT OF INTEREST

The authors hereby declare that there is no conflict of interest.

REFERENCES

- [1] A. Aravind, M. Jayaraj, M. Kumar, R. Chandra, Optical and magnetic properties of copper doped ZnO nanorods prepared by hydrothermal method, *Journal of Materials Science: Materials in Electronics*, 24 (2013) 106-112. <https://doi.org/10.1007/s10854-012-0911-6>
- [2] I. Ayoub, V. Kumar, R. Abolhassani, R. Sehgal, V. Sharma, R. Sehgal, H.C. Swart, Y.K. Mishra, *Advances in ZnO: Manipulation of defects for enhancing their technological potentials*, *Nanotechnology Reviews*, 11 (2022) 575-619. <https://doi.org/10.1515/ntrev-2022-0035>
- [3] Y.-L. Chu, S.-J. Young, L.-W. Ji, T.-T. Chu, P.-H. Chen, Synthesis of Ni-doped ZnO nanorod arrays by chemical bath deposition and their application to nanogenerators, *Energies*, 13 (2020) 2731. <https://doi.org/10.3390/en13112731>
- [4] A. Shokri, M. Salimi, T. Abmatin, Employing photo Fenton and UV/ZnO processes for removing Reactive red 195 from aqueous environment, *Fresenius Environmental Bulletin*, 26 (2017) 1560-1565.
- [5] A. Shokri, K. Mahanpoor, Using UV/ZnO process for degradation of Acid red 283 in synthetic wastewater, *Bulgarian Chemical Communications*, 50 (2018) 27-32.
- [6] R. Hekmatshoar, A.R. Yari, A. Shokri, Using ZnO based on Bentonite as a nano photocatalyst for degradation of Acid Red 114 in synthetic wastewater, *Journal of Nanoanalysis*, 7 (2020) 282-292.
- [7] Z.L. Wang, X. Kong, J. Zuo, Induced growth of asymmetric nanocantilever arrays on polar surfaces, *Physical Review Letters*, 91 (2003) 185502. <https://doi.org/10.1103/PhysRevLett.91.185502>
- [8] Y. Zhang, X. Song, J. Zheng, H. Liu, X. Li, L. You, Symmetric and asymmetric growth of ZnO hierarchical nanostructures: nanocombs and their optical properties, *Nanotechnology*, 17 (2006) 1916. <https://doi.org/10.1088/0957-4484/17/8/019>
- [9] A.K. Rana, Y. Kumar, N. Saxena, R. Das, S. Sen, P.M. Shirage, Studies on the control of ZnO nanostructures by wet chemical method and plausible mechanism, *AIP Advances*, 5 (2015) 097118. <https://doi.org/10.1063/1.4930598>
- [10] B. LeRoy, S. Lemay, J. Kong, C. Dekker, Scanning tunneling spectroscopy of suspended single-wall carbon nanotubes, *Applied physics letters*, 84 (2004) 4280-4282. <https://doi.org/10.1063/1.1748836>
- [11] Y. Kumar, A.K. Rana, P. Bhojane, M. Pusty, V. Bagwe, S. Sen, P.M. Shirage, Controlling of ZnO nanostructures by solute concentration and its effect on growth, structural and optical properties, *Materials Research Express*, 2 (2015) 105017. <https://doi.org/10.1088/2053-1591/2/10/105017>
- [12] Z.L. Wang, X.Y. Kong, Y. Ding, P. Gao, W.L. Hughes, R. Yang, Y. Zhang, Semiconducting and piezoelectric oxide nanostructures induced by polar surfaces, *Advanced Functional Materials*, 14 (2004) 943-956. <https://doi.org/10.1002/adfm.200400180>
- [13] Y. Heo, D. Norton, L. Tien, Y. Kwon, B. Kang, F. Ren, S. Pearton, J. LaRoche, ZnO nanowire growth and devices, *Materials Science and Engineering: R: Reports*, 47 (2004) 1-47. <https://doi.org/10.1016/j.mser.2004.09.001>
- [14] P.M. Shirage, ZnO nano-flowers, *Mater. Today*, 16 (2013) 505-506. <https://doi.org/10.1016/j.mattod.2013.11.007>
- [15] F. Ahmed, N. Arshi, M. Anwar, R. Danish, B.H. Koo, Mn-doped ZnO nanorod gas sensor for oxygen detection, *Current Applied Physics*, 13 (2013) S64-S68. <https://doi.org/10.1016/j.cap.2012.12.029>
- [16] O. Alev, İ. Ergün, O. Oezdemir, L.C. Arslan, S. Büyükköse, Z.Z. Öztürk, Enhanced ethanol sensing performance of Cu-doped ZnO nanorods, *Materials Science in Semiconductor Processing*, 136 (2021) 106149. <https://doi.org/10.1016/j.mssp.2021.106149>
- [17] O. Alev, N. Sarıca, O. Özdemir, L.C. Arslan, S. Büyükköse, Z.Z. Öztürk, Cu-doped ZnO nanorods based QCM sensor for hazardous gases, *Journal of Alloys and Compounds*, 826 (2020) 154177. <https://doi.org/10.1016/j.jallcom.2020.154177>
- [18] M. Asemi, B. Mortezaipoor, M. Ghanaatshoar, Structural, Optical, and Magnetic Properties of Hydrothermally Grown Fe-Doped ZnO Nanorod Arrays on Glass Substrate, *Journal of Superconductivity and Novel Magnetism*, 32 (2019) 269-275. <https://doi.org/10.1007/s10948-018-4946-7>
- [19] X. Wu, Z. Wei, L. Zhang, C. Zhang, H. Yang, J. Jiang, Synthesis and characterization of Fe and Ni co-doped ZnO nanorods synthesized by a hydrothermal method, *Ceramics International*, 40 (2014) 14635-14640. <https://doi.org/10.1016/j.ceramint.2014.06.050>
- [20] A. Shokri, Using Mn based on lightweight expanded clay aggregate (LECA) as an original catalyst for the removal of NO₂ pollutant in aqueous environment, *Surfaces and Interfaces*, 21 (2020) 100705. <https://doi.org/10.1016/j.surfin.2020.100705>
- [21] A. Shokri, Using NiFe₂O₄ as a nano photocatalyst for degradation of polyvinyl alcohol in synthetic wastewater, *Environmental Challenges*, 5 (2021) 100332. <https://doi.org/10.1016/j.envc.2021.100332>
- [22] A. Shokri, K. Mahanpoor, Removal of Ortho-Toluidine from Industrial Wastewater by UV/TiO₂ Process, *Journal of Chemical Health Risks*, 6 (2016) -.
- [23] T. Bhuyan, M. Khanuja, R. Sharma, S. Patel, M. Reddy,



- S. Anand, A. Varma, A comparative study of pure and copper (Cu)-doped ZnO nanorods for antibacterial and photocatalytic applications with their mechanism of action, *Journal of Nanoparticle Research*, 17 (2015) 1-11. <https://doi.org/10.1007/s11051-015-3093-3>
- [24] K. Godini, M. Tahergorabi, M. Naimi-Joubani, M. Shirzad-Siboni, J.-K. Yang, Application of ZnO nanorods doped with Cu for enhanced sonocatalytic removal of Cr (VI) from aqueous solutions, *Environmental Science and Pollution Research*, 27 (2020) 2691-2706. <https://doi.org/10.1007/s11356-019-07165-9>
- [25] S. N Sarangi, V. Siva, B. K Padhi, P. K Sahoo, Synthesis of Cu doped ZnO nanorods for photosensitive UV detection application, *Advanced Materials Letters*, 8 (2017) 524-530. <https://doi.org/10.5185/amlett.2017.7022>
- [26] S. Narasimman, L. Balakrishnan, Z. Alex, Fiber optic magnetic field sensor using Co doped ZnO nanorods as cladding, *RSC advances*, 8 (2018) 18243-18251. <https://doi.org/10.1039/C8RA01803K>
- [27] R. Shabannia, High-sensitivity UV photodetector based on oblique and vertical Co-doped ZnO nanorods, *Materials Letters*, 214 (2018) 254-256. <https://doi.org/10.1016/j.matlet.2017.12.019>
- [28] W. Wang, F. Zhang, X. Wang, S. Zhang, J. Yan, W. Zhang, W. Zhang, Magnetic and optical properties of Co-doped ZnO nanorod arrays, *The European Physical Journal Plus*, 135 (2020) 1-14. <https://doi.org/10.1140/epjp/s13360-019-00086-z>
- [29] A.K. Rana, P. Bankar, Y. Kumar, M.A. More, D.J. Late, P.M. Shirage, Synthesis of Ni-doped ZnO nanostructures by low-temperature wet chemical method and their enhanced field emission properties, *RSC advances*, 6 (2016) 104318-104324. <https://doi.org/10.1039/C6RA21190A>
- [30] Y.-L. Chu, S.-J. Young, L.-W. Ji, I.-T. Tang, T.-T. Chu, Fabrication of ultraviolet photodetectors based on Fe-doped ZnO nanorod structures, *Sensors*, 20 (2020) 3861. <https://doi.org/10.3390/s20143861>
- [31] A. Ismail, M. Mamat, I.S. Banu, R. Amiruddin, M. Malek, N. Parimon, A. Zoolfakar, N.M. Sin, A. Suriani, M. Ahmad, Structural modification of ZnO nanorod array through Fe-doping: ramification on UV and humidity sensing properties, *Nano-Structures & Nano-Objects*, 18 (2019) 100262. <https://doi.org/10.1016/j.nanoso.2019.100262>
- [32] N.D. Raskar, D.V. Dake, V.A. Mane, E. Stathatos, U. Deshpande, B. Dole, One step synthesis of vertically grown Mn-doped ZnO nanorods for photocatalytic application, *Journal of Materials Science: Materials in Electronics*, 30 (2019) 10886-10899. <https://doi.org/10.1007/s10854-019-01433-7>
- [33] M. Chakraborty, A. Ghosh, R. Thangavel, Experimental and theoretical investigations of structural and optical properties of copper doped ZnO nanorods, *Journal of Sol-Gel Science and Technology*, 74 (2015) 756-764. <https://doi.org/10.1007/s10971-015-3660-1>
- [34] M. Tosun, S. Senol, L. Arda, Effect of Mn/Cu co-doping on the structural, optical and photocatalytic properties of ZnO nanorods, *Journal of Molecular Structure*, 1212 (2020) 128071. <https://doi.org/10.1016/j.molstruc.2020.128071>
- [35] R. Torkamani, B. Aslibeiki, H. Naghsara, M. Darbandi, Structural and optical properties of ZnO nanorods: The effect of concentration and pH of the growth solution, *Optical Materials*, 127 (2022) 112295. <https://doi.org/10.1016/j.optmat.2022.112295>
- [36] M. Abdelfatah, H. Salah, M. El-Henawey, A. Oraby, A. El-Shaer, W. Ismail, Insight into Co concentrations effect on the structural, optical, and photoelectrochemical properties of ZnO rod arrays for optoelectronic applications, *Journal of Alloys and Compounds*, 873 (2021) 159875. <https://doi.org/10.1016/j.jallcom.2021.159875>
- [37] G. Murugadoss, Synthesis and characterization of transition metals doped ZnO nanorods, *Journal of Materials Science & Technology*, 28 (2012) 587-593. [https://doi.org/10.1016/S1005-0302\(12\)60102-9](https://doi.org/10.1016/S1005-0302(12)60102-9)
- [38] A.C. Ekennia, D.N. Uduagwu, N.N. Nwaji, O.O. Oje, C.O. Emma-Uba, S.I. Mgbii, O.J. Olowo, O.L. Nwanji, Green synthesis of biogenic zinc oxide nanoflower as dual agent for photodegradation of an organic dye and tyrosinase inhibitor, *Journal of Inorganic and Organometallic Polymers and Materials*, 31 (2021) 886-897. <https://doi.org/10.1007/s10904-020-01729-w>

